Plasma Physics and Controlled Fusion, Vol. 34, No. 6, pp. 1133 to 1156, 1992
Printed in Great Britain.

0741-3335/92 $5.00+ .00
IOP Publishing Ltd. and Pergamon Press Ltd.

DIFFRACTION ANALYSIS OF FORWARD-ANGLE SCATTERING IN PLASMAS

J. HOWARD and L. E. SHARP
Plasma Research Laboratory, Research School of Physical Sciences, Australian National University, Canberra, A.C.T. 2601, Australia

(*Received* 14 *August* 1991)

Abstract—A scalar diffraction treatment of forward-angle laser scattering diagnostics (e.g. scintillation interferometry, far-forward scattering) is presented. Results obtained by other workers for Gaussian beam scattering from plasma waves are generalized for arbitrary weakly scattering media and for both near-field (imaging) and far-field (focal plane) experimental configurations. Essential elements of the theory have been confirmed by near-field experimental measurements on airborne ultrasound.

1. INTRODUCTION

LINE-OF-SIGHT MEASUREMENT of the plasma refractive index (forward-angle scattering, interferometry, shadowgraphy etc.) is a powerful diagnostic for both the short-scale random components of the plasma density distribution as well as the long-wavelength coherent structures (e.g. JACOBSON, 1982; YOUNG *et al.*, 1984; HOWARD *et al.*, 1987; NAZIKIAN and SHARP, 1987; KIM *et al.*, 1988; WEISEN *et al.*, 1988). In this work, an analysis of the diffraction of a Gaussian laser beam from a weakly perturbing, but otherwise arbitrary refractive index distribution, valid throughout the diffraction region is presented. The implications for interferometric and small-angle scattering experiments in near, Fresnel (intermediate) and far-field limits are examined. The far-field small-angle description of scattering from waves given by EVANS *et al.* (1982) is generalized to arbitrary refractive structures, reducing to the Evans expressions for harmonic disturbances. The work, however, highlights the properties of near-field techniques which have the advantage of conveying the transverse spectral features of the medium with little or no distortion. In addition, measurements in the Fresnel region allow some line-of-sight resolution of the scattering source distribution. Experimental scintillation measurements confirming these expectations are reported here.

Section 2 reviews the relevant aspects of scalar electromagnetic diffraction theory introducing both Rytov and Born perturbation solutions to the wave equation for weakly fluctuating media. Our starting point is the *diffraction projection theorem* (WOLF, 1969), which is the wavenumber domain solution to the scalar inhomogeneous wave equation in the Born approximation. It is the Rytov approach (e.g. STROHBEHN, 1968), however, that proves the more natural framework for the analysis of forward-angle, scattering techniques. An expression for the perturbed complex *Rytov phase* for the ideal case of plane-wave illumination is obtained, and shown to transform simply (in the paraxial approximation) under the action of a collecting optic. The theory is readily extended to Gaussian beams in Section 3 to yield a general expression for laser-beam scattering from an arbitrary medium in the region beyond the plasma, with or without a thin collecting optic. In Section 4, it is shown that the signals obtained using optical mixing detection (e.g. heterodyne detection) are related linearly

to the perturbed Rytov phase. Limiting expressions for the far-field (focal plane) and near-field (imaging) detector signals are then derived in Sections 5 and 6. Finally, in Section 7, we report near- and intermediate-field interferometry experiments on airborne ultrasound that support the theoretical results. It is demonstrated that a thin coherent disturbance can be localized from near-field measurements of the complex Rytov phase.

2. SCALAR DIFFRACTION THEORY

We consider propagation in the z direction of a monochromatic wave ($\omega_0 = ck_0$, $k_0 = 2\pi/\lambda_0$) of arbitrary spatial distribution through an inhomogeneous, weakly perturbing plasma. The coordinate origin (incident plane) is chosen so that the plasma occupies the region $0 < z' < L$, and the measurement plane is located beyond the plasma ($z' > L$). The diffraction geometry for the ideal case of an incident plane wave is illustrated in Fig. 1. The propagation of the incident wave is determined by the refractive index $1+n(\mathbf{R}', t)$ where $\mathbf{R}' = (x', y', z')$ is a point in the plasma. For sufficiently high frequencies the deviation from vacuum is a scalar quantity

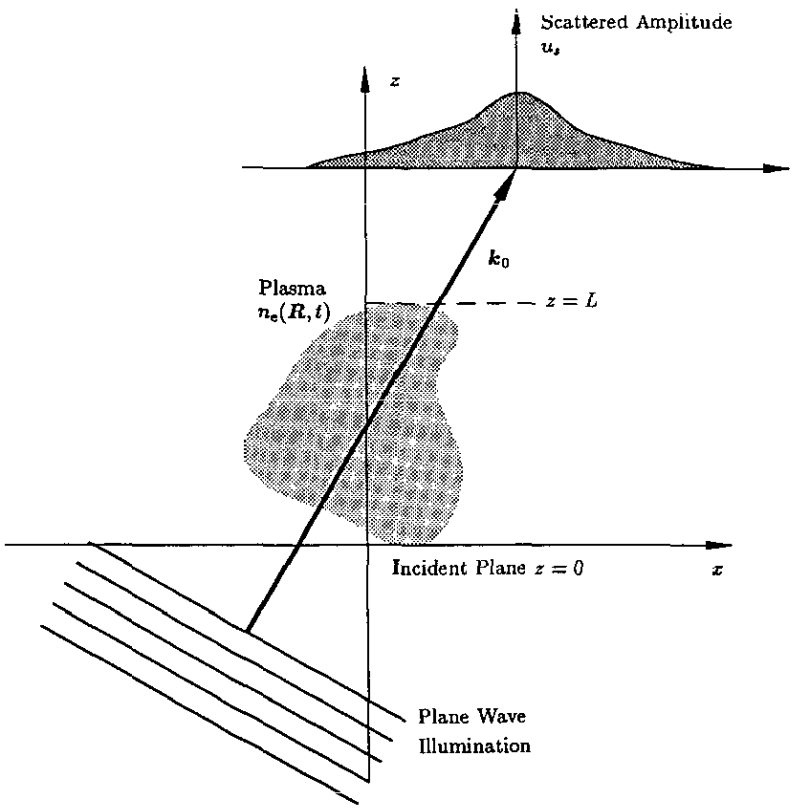

FIG. 1.—Diffraction geometry for the case of incident plane-wave illumination of the plasma. The scattered wave field is measured in some arbitrary plane z.

$n(\mathbf{R}', t) = -n_e(\mathbf{R}', t)/2n_{cr}$ where $n_e(\mathbf{R}', t)$ is the electron density, $n_{cr} = k_0^2/(4\pi r_e)$ is the critical density and r_e is the classical electron radius. For small scattering angles, depolarization of the incident wave can be ignored and the electric field treated as a scalar quantity (e.g. CLIFFORD, 1978; SURKO and SLUSHER, 1980). The total scalar field $u(\mathbf{R}, t)$ at some point $\mathbf{R} = (x, y, z)$ outside the plasma can be regarded as the sum of the incident $u_0(\mathbf{R}, t)$ and scattered waves $u_s(\mathbf{R}, t)$. Below we summarize the properties of these component fields in turn.

2.1. *The incident field*

The free-space field satisfies the scalar homogeneous Helmholtz equation

$$(\nabla^2 + k_0^2)u_0 = 0 \tag{2.1}$$

the solution to which is most conveniently obtained in the wavenumber domain (GOODMAN, 1968). The incident wave field has angular spectrum

$$A(\boldsymbol{\kappa}_\perp, \omega; 0) = \int_{-\infty}^{\infty} \mathrm{d}t\, \mathrm{d}\boldsymbol{\rho} u_0(\boldsymbol{\rho}; 0, t) \exp\left[-j(\boldsymbol{\kappa}_\perp \cdot \boldsymbol{\rho} - \omega t)\right] \tag{2.2}$$

where $\boldsymbol{\rho} = (x, y)$ denotes a vector in the incident plane $z = 0$, $\mathrm{d}\boldsymbol{\rho} = \mathrm{d}x\, \mathrm{d}y$, $\boldsymbol{\kappa} = (\boldsymbol{\kappa}_\perp, \kappa_z)$ and $\boldsymbol{\kappa}_\perp$ is a two-dimensional wavenumber. For a monochromatic wave we write $A(\boldsymbol{\kappa}_\perp, \omega; 0) = 2\pi A_0(\boldsymbol{\kappa}_\perp; 0)\delta(\omega - \omega_0)$ where δ is the Dirac delta function. Satisfaction of the Helmholtz equation requires that the Fourier amplitudes propagate according to

$$A_0(\boldsymbol{\kappa}_\perp; z) = \mathscr{H}(\kappa_z; z) A_0(\boldsymbol{\kappa}_\perp; 0) \tag{2.3}$$

where

$$\mathscr{H}(\kappa_z; z) = \exp(j\kappa_z z) \tag{2.4}$$

is the free-space transfer function or propagator for the unperturbed beam (SHEWELL and WOLF, 1968) and $\kappa_z = (k_0^2 - \mathbf{k}_\perp^2)^{1/2}$. For $|\boldsymbol{\kappa}_\perp| > k_0$, κ_z is imaginary and the wave is evanescent. The field at an arbitrary plane z can be expressed in terms of the incident field by taking the inverse Fourier transform of equation (2.3) to obtain

$$u_0(\mathbf{R}, t) = \int_{-\infty}^{\infty} \mathrm{d}\boldsymbol{\rho}' u_0(\mathbf{R}', t) h(\mathbf{R} - \mathbf{R}') \tag{2.5}$$

with free-space kernel

$$h(\mathbf{R}) = \int_{-\infty}^{\infty} \frac{\mathrm{d}\boldsymbol{\kappa}_\perp}{(2\pi)^2} \exp(j\boldsymbol{\kappa} \cdot \mathbf{R}). \tag{2.6}$$

For small scattering angles, κ_z in equation (2.4) can be approximated to second order by

$$\kappa_z \approx \kappa_F \equiv k_0 + k_F \tag{2.7}$$

where $k_F = -\boldsymbol{\kappa}_\perp^2/2k_0 = -2\pi/z_F$ and z_F is the Fresnel length. The approximation is valid provided that the residual phase $\kappa_\perp^4 z/8k_0^3$, $\kappa_\perp = |\boldsymbol{\kappa}_\perp|$ is negligible. With $\mathscr{H}$ replaced by its parabolic (or Fresnel) approximation $\mathscr{H}_F$ (obtained by setting $\kappa_z = \kappa_F$ in the exponent), the convolution theorem again recovers equation (2.5) but with Fresnel kernel

$$h_F(\boldsymbol{\rho}, z) = \frac{\exp(jk_0 z)}{j\lambda_0 z} \exp\left(\frac{jk_0}{2z}\rho^2\right). \tag{2.8}$$

2.2 *The diffracted field*

In the radiation zone ($k_0|\mathbf{R}-\mathbf{R}'| \gg 1$) and in the "low-temperature" approximation (SHEFFIELD, 1975), the scattered component satisfies the inhomogeneous Helmholtz equation

$$(\nabla^2 + k_0^2)u_s(\mathbf{R}, t) = f(\mathbf{R}, t) \tag{2.9}$$

where

$$f(\mathbf{R}, t) = -2k_0^2 n(\mathbf{R}, t)u(\mathbf{R}, t) \tag{2.10}$$

is the scalar scattering potential. The solution, obtained using Green's function techniques, is an integral equation containing the unknown scattered component u_s on both sides. A closed expression, therefore, does not generally exist. Nevertheless, provided $n = -n_e/2n_{cr}$† is small (in a sense to be defined) an approximate explicit solution can be found using either an additive (Born) or multiplicative (Rytov) perturbation technique. In the Born approximation, the wave field is expanded in series form

$$u = u_0 + u_1 + u_2 + \cdots \tag{2.11}$$

and only terms up to first-order are retained. Neglect of the second-order term $-2k_0^2 n u_1$ in the perturbed wave equation is valid provided that $|u_1/u_0| \lesssim n$. To interpret this approximation, we consider the wave to be normally incident upon a plasma "blob" of dimension $\sim\Lambda$. The difference in phase between the incident (u_0) and transmitted (u_0+u_s) beams is $\Delta\phi = (\kappa - k_0)\Lambda$ where $\kappa \sim k_0(1+n)$ is the wavenumber in the plasma. In order that u_s be small we must have $\Delta\phi \ll \pi$ requiring that $n \ll K/k_0$ where $K = 2\pi/\Lambda$. The maximum tolerable density perturbation therefore depends upon the dimension of the inhomogeneity. The total Born field is $u_B = u_0 + u_s$ where $u_s = u_1$ is given by

$$u_s(\mathbf{R}, t) = \int_{-\infty}^{\infty} d\mathbf{R}'\, f_0(\mathbf{R}', t) g(\mathbf{R}-\mathbf{R}') \tag{2.12}$$

† Hereafter simply the "density".

where

$$g(\mathbf{R}) = \frac{-\exp(jk_0|\mathbf{R}|)}{4\pi|\mathbf{R}|} \tag{2.13}$$

is the Green's function and $f_0(\mathbf{R}', t)$ is identical to equation (2.10) but for the replacement of the total field $u(\mathbf{R}', t)$ by the unperturbed field $u_0(\mathbf{R}', t)$. Note the duality between equation (2.12) and its vacuum counterpart equation (2.5). The integral expansion for the Green's function [cf. equation (A.1)] is also similar to equation (2.6) for the free-space kernel.

The diffraction projection theorem (see also the Appendix) is the wavenumber space solution to the inhomogeneous Helmholtz equation obtained in the Born approximation. In close affinity with the free-space result equation (2.3), it relates the angular spectrum A_s of the scattered radiation to the three-dimensional Fourier transform F_0 of the scattering potential on a hemispherical surface in the spatial frequency domain:

$$A_s(\boldsymbol{\kappa}_\perp, \omega; z) = \mathscr{G}(\kappa_z; z) F_0(\boldsymbol{\kappa}, \omega). \tag{2.14}$$

Apart from an imaginary factor, the transfer function $\mathscr{G}$ is the same as the free space propagator $\mathscr{H}$ [equation (2.4)]:

$$\mathscr{G}(\kappa_z; z) = \frac{j}{\kappa_z} \exp(j\kappa_z z). \tag{2.15}$$

As $0 < |\boldsymbol{\kappa}_\perp| < k_0$ (propagating components), the vector $\boldsymbol{\kappa}$ is constrained to the hemispherical surface in reciprocal space that is centered on the origin and has radius k_0. This is a consequence of momentum conservation for elastic scattering ($|\boldsymbol{\kappa}| = k_0$). The parabolic approximation to equation (2.14) is obtained by replacing $\kappa_z = \kappa_F$ and $\kappa_z = k_0$ in the denominator of $\mathscr{G}$ and is equivalent to the familiar spatial-domain Fresnel approximation to the Green's function.

For an incident plane wave $u_0 = a_0 \exp[j(\mathbf{k}_0 \cdot \mathbf{R} - \omega_0 t)]$, $\mathbf{k}_0 = (k_{0x}, k_{0y}, k_{0z})$ equation (2.14) reduces to the form first presented by WOLF (1969):

$$A_P(\boldsymbol{\kappa}_\perp, \omega; z) = \mathscr{G}(\kappa_z; z) F_P(\mathbf{K}, \Omega) \tag{2.16}$$

where

$$\mathbf{K} \equiv (\boldsymbol{\kappa}, k_z) = \boldsymbol{\kappa} - \mathbf{k}_0 \tag{2.17}$$

$$\Omega = \omega - \omega_0 \ll \omega_0 \tag{2.18}$$

and $F_P(\mathbf{K}, \Omega) = -2k_0^2 a_0 N(\mathbf{K}, \Omega)$ is the transform of the plane-wave scattering potential. Taking $\mathbf{k}_0 = (0, 0, k_0)$, the relation in the transform plane $(k_x, 0, k_z)$ is illustrated

in Fig. 2. The forward-scattered wave vector $\boldsymbol{\kappa}$ lies on a hemisphere that passes through the origin and has centre $(0, 0, -k_{0z})$. The axis of the hemisphere is in a direction normal to the measurement plane. The scattering angle θ_s is given by the familiar Bragg relation $\sin(\theta_s/2) = K/2k_0$, $K = |\mathbf{K}|$.

In the Rytov approximation, it is the exponent of u that is developed as a series:

$$u = \exp(\psi_0 + \psi_1 + \psi_2 + \cdots). \tag{2.19}$$

A solution for the first-order complex phase $\psi_1 = \chi_1 + j\varphi_1$ is obtained by applying the Rytov transformation to the wave equation and neglecting terms of order $(\nabla\psi_1)^2 \ll k_0^2 n$ (STROHBEHN, 1968). Observe that χ_1 and φ_1 represent respectively the amplitude and phase perturbations suffered by the beam on passage through the plasma. For our plasma "blob" we have $|\nabla\psi_1| \sim \Delta\varphi_1/\Lambda$ and the approximation is valid provided $n \ll 1$. Unlike the first-order Born approximation, this condition on n is independent of the scale size of the inhomogeneities. For forward-angle scattering applications, and especially interferometry, where the condition $K/k_0 < 1$ is strongly satisfied, the Rytov approximation would appear to be superior to its Born counterpart. A useful comparison of the limitations of the two approximations is given by SLANEY *et al.* (1984). In the first-order Rytov approximation ($\psi_s = \chi_s + j\varphi_s = \psi_1$) the total scattered field is $u_R = u_0 \exp(\psi_s)$ where the incident wave $u_0 = \exp(\psi_0)$ satisfies equation (2.1) and the solution for the perturbed Rytov phase can be obtained as (DEVANEY, 1986):

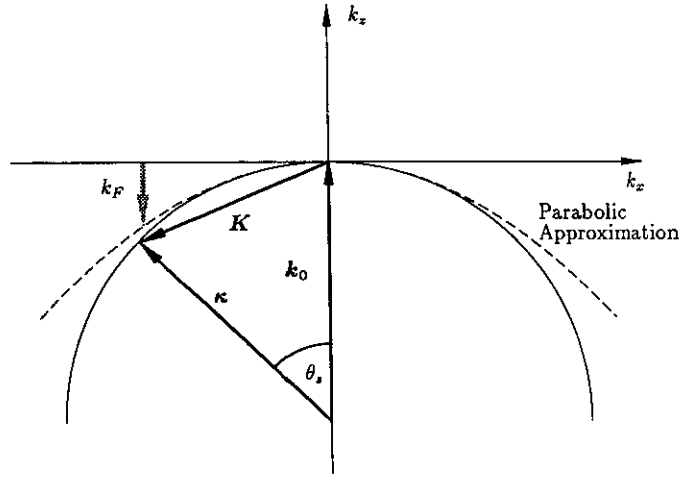

FIG. 2.—Schematic diagram showing wave vector matching for elastic scattering together with the parabolic approximation to the semi-circular arc in the region of the origin for the case of incident plane-wave illumination $\mathbf{k}_0 = (0, 0, k)$. The shaded arrow is the Fresnel approximation to the wavenumber component k_z.

$$\psi_s(\mathbf{R}, t) = \frac{u_s(\mathbf{R}, t)}{u_0(\mathbf{R}, t)} \tag{2.20}$$

$$= -2k_0^2 \int_{-\infty}^{\infty} d\mathbf{R}' n(\mathbf{R}', t) \exp[\psi_0(\mathbf{R}', t) - \psi_0(\mathbf{R}, t)] g(\mathbf{R} - \mathbf{R}'). \tag{2.21}$$

The three terms in the integrand represent respectively the influence of the medium, the incident beam properties and the propagation behaviour. The first-order Rytov solution ψ_s is thus constructed from the Born solution equation (2.12) through the relation (2.20). Expressions for ψ_s valid in the parabolic approximation are developed in the Appendix.

For the special case of plane wave illumination, a simple result, analogous to the diffraction projection theorem [equation (2.16)], follows for the Fourier transform of the Rytov phase:

$$\Psi_P(\mathbf{k}, \Omega; z) = \mathscr{R}(k_z; z) N(\mathbf{K}, \Omega) \tag{2.22}$$

where

$$\mathscr{R}(k_z; z) = \frac{jk_0^2}{k_z} \exp(jk_z z) \tag{2.23}$$

is the Rytov phase propagator. In principle A_P (or Ψ_P) can yield information about the electron density distribution to a bandlimit $2k_0$. The condition under which equation (2.12) and hence the results (2.14) and (2.21) are valid, however, requires the scattering angles to be small enough that the scalar theory is valid. In this context, the spatially apodizing effects and diffraction of finite diameter probing beams also need to be addressed. In Section 3 we therefore examine the Rytov phase for Gaussian beam scattering in the parabolic approximation. It is convenient to use the Rytov formalism because of the amenable properties of the Gaussian beam Rytov phase $\psi_G = \chi_G + j\varphi_G$ in the plane-wave and collimated-beam limits, and because of the simple relationship between ψ_G and the signals measured using heterodyne and homodyne detection systems. For imaging (or focal-plane) scattering experiments it is necessary, however, to first construct an expression for the Rytov phase in front of a collecting optic.

2.3. *Effect of a lens*

We consider a lens of focal length f at distance d_0 from the disturbance ($z = L$) and calculate the field u_s in the detection plane $z = L + d_0 + d_1$ at distance d_1 in front of the lens. The special case when the detector resides in the image plane of the field diffracted from a thin phase disturbance is illustrated in Fig. 3. For collimated laser beams and small scattering angles it is reasonable to assume that the optic collects all of the scattered radiation. The action of an infinite aperture thin lens in the parabolic approximation is to produce a Fresnel transform

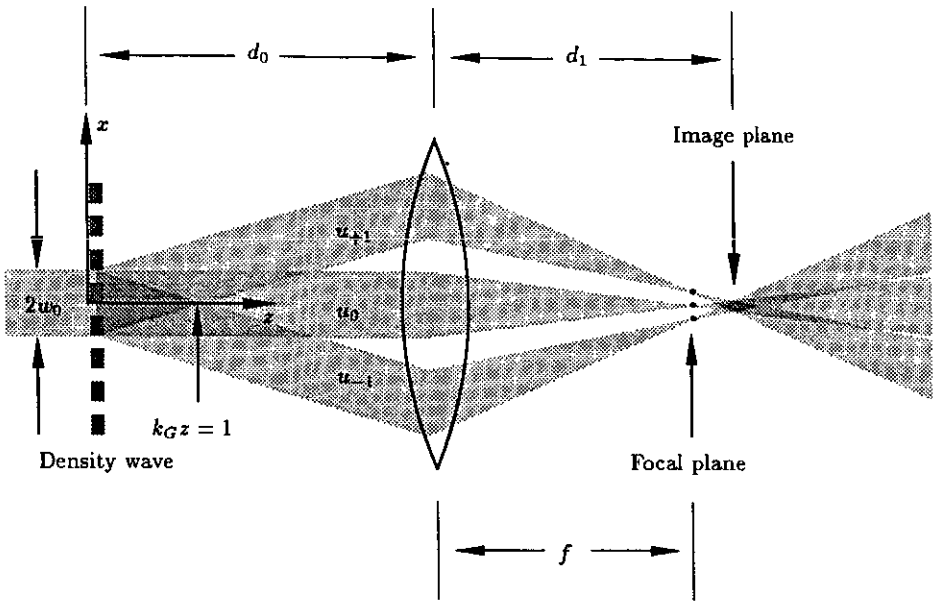

FIG. 3.—Schematic diagram showing collimated Gaussian-beam diffraction from a thin-density wave for the case when the detector resides in the image plane.

$$u_\alpha(\boldsymbol{\rho}, z, t) = \int_{-\infty}^{\infty} \mathrm{d}\boldsymbol{\rho}' h_\alpha(\boldsymbol{\rho}', \boldsymbol{\rho}, d_0, d_1) u_R(\boldsymbol{\rho}', L, t). \tag{2.24}$$

The lens kernel h_α is related to the Fresnel kernel by

$$h_\alpha(\boldsymbol{\rho}', \boldsymbol{\rho}, d_0, d_1) = \alpha \exp(j\phi_\alpha) h_F(\boldsymbol{\rho}' - \alpha\boldsymbol{\rho}, d_0 + \alpha d_1) \tag{2.25}$$

where $\phi_\alpha = -(k_0\alpha/2f)(\boldsymbol{\rho}_1^2 + 2a_1^2)$ is a fixed-phase curvature and

$$\alpha = 1/(1 - d_1/f) \tag{2.26}$$

is the *lens parameter*. Recalling that the propagation of the Rytov field $u_R = \exp(\psi_0 + \psi_s)$ is governed by the Fresnel integral, and expressing the field in the detection plane z as $u_\alpha = \exp(\psi_{\alpha 0} + \psi_\alpha)$, comparison of equations (2.24) and (2.5) reveals that

$$\psi_\alpha(\mathbf{R}, t) = \psi_s(\hat{\mathbf{R}}, t) \tag{2.27}$$

where

$$\hat{\mathbf{R}} = (\alpha\boldsymbol{\rho}, z + (\alpha - 1)d_1). \tag{2.28}$$

The scaling and quadratic phase terms are absorbed by the unperturbed phase

$\psi_{\alpha 0} = \psi_0 + (\ln \alpha + j\phi_\alpha)$. The Rytov phase in front of the lens can thus be obtained from ψ_s and the measurement geometry using a linear coordinate transformation.

The character of the "lens" Rytov phase ψ_α is determined by α. For example, when $f \to \infty$ then $\alpha = 1$ and the lens-free result is recovered. The Fourier transforming property of the lens for the field in the front focal plane is obtained in the limit $d_1 = f$, $\alpha \to \infty$ and is discussed in Section 5. Substituting the imaging condition $\alpha = -d_0/d_1 = -1/M$ gives $\psi_\alpha = \psi_G(-\boldsymbol{\rho}/M, L, t)$ which is identical apart from inversion and magnification by M to the Rytov phase in the plane L. Imaging techniques are particularly useful for restoring near field conditions (see Section 6) at a remote measurement plane.

3. GAUSSIAN BEAMS

The Gaussian-beam Rytov phase can be obtained from the plane-wave phase by means of a coordinate transformation. We assume a probing Gaussian beam coincident with the z-axis with beam waist located at z_0, and take the y-axis to point in the toroidal direction. The transverse and longitudinal coordinates are normalized to the beam waist dimension w_0 [radius at exp (-1) of the power profile] and Rayleigh length $z_R = k_0 w_0^2$, respectively:

$$\mathbf{u} = \frac{\boldsymbol{\rho}}{w_0} \quad \mathbf{v} = \mathbf{k} w_0 \tag{3.1}$$

$$\zeta = \frac{z}{z_R} \quad \zeta' = \frac{z'}{z_R} \quad \zeta_0 = \frac{z_0}{z_R} \quad l = \frac{L}{z_R}. \tag{3.2}$$

Propagating the Gaussian plane wave at the waist position ζ_0 to the plane ζ using the Fresnel integral allows the free-space field to be written as $u_{G0} = \exp(\psi_{G0})$ with complex phase

$$\psi_{G0}(\mathbf{u}, \zeta, t) = c_G - \frac{\mathbf{u}^2}{2\gamma} + j[k_0 z_R \zeta - \omega_0 t] \tag{3.3}$$

where

$$\gamma = 1 + j(\zeta - \zeta_0) \tag{3.4}$$

$$c_G = \ln\left(\frac{a_0}{\pi w_0 |\gamma|}\right) - j \tan^{-1}(\zeta - \zeta_0) \tag{3.5}$$

and the beam power a_0^2 is, for convenience, taken as unity. Equation (3.3) is valid provided the parabolic condition $\zeta \ll (k_0 w_0)^2$ is satisfied. Substituting equation (3.3) in equation (A.8) for the parabolically approximated ψ_s readily yields the first-order Gaussian-beam Rytov phase:

$$\psi_G(\mathbf{u},\zeta,t) = jk_0 z_R \int_0^l d\zeta' \int_{-\infty}^{\infty} \frac{d\mathbf{v}}{(2\pi)^2} \mathscr{D}_\psi(\mathbf{v};\mathbf{u},\zeta,\zeta') N(\mathbf{v};\zeta',t) \tag{3.6}$$

with kernel

$$\mathscr{D}_\psi(\mathbf{v};\mathbf{u},\zeta,\zeta') = \exp\{j\beta[\mathbf{u}\cdot\mathbf{v}+v_F(\zeta-\zeta')]\} \tag{3.7}$$

where $v_F = -v^2/2$ and

$$\beta = \gamma'/\gamma \quad \gamma' = 1+j(\zeta'-\zeta_0). \tag{3.8}$$

The two-dimensional refractive index transform has the normalization $N(\mathbf{v};\zeta',t) = N(\mathbf{k};z',t)/w_0^2$. Analogous expressions to equation (3.6) apply for the real (amplitude) and imaginary (phase) parts of ψ_G with kernels

$$\left.\begin{matrix} 2\mathscr{D}_\chi(\mathbf{v};\mathbf{u},\zeta,\zeta') \\ 2j\mathscr{D}_\varphi(\mathbf{v};\mathbf{u},\zeta,\zeta') \end{matrix}\right\} = \mathscr{D}_\psi(\mathbf{v};\mathbf{u},\zeta,\zeta') \mp \mathscr{D}_\psi^*(-\mathbf{v};\mathbf{u},\zeta,\zeta'). \tag{3.9}$$

The kernels fold in effects due both to diffraction from plasma irregularities and spreading of the finite-diameter probing beam.

The plane-wave Rytov phase ψ_P [obtained by inverse Fourier transformation of equation (2.22)] is recovered in the limit $\beta \to 1$. When the interaction region is narrow compared with the Rayleigh range ($l \to 0$), the parameter $\beta \to \bar{\beta}$ can be taken as independent of the plasma coordinate ζ' and ψ_G obtained from the plane-wave phase ψ_P through the coordinate transformation:

$$\psi_G(\mathbf{u},\zeta,t) = \psi_P(\bar{\beta}\mathbf{R},t) \tag{3.10}$$

where, of course, $\mathbf{R} = (w_0\mathbf{u}, z_R\zeta)$. The Gaussian-beam Rytov phase for diffraction from a thin phase screen and in front of a collecting optic is obtained by combining equations (2.27) and (3.10):

$$\psi_\alpha(\mathbf{R},t) = \psi_P[\alpha\bar{\beta}\boldsymbol{\rho}, \bar{\beta}z+(\alpha-1)d_1, t]. \tag{3.11}$$

This expression is used below to calculate the scattered signals from airborne ultrasound for comparison with experiment.

4. DETECTION

We now relate the total Gaussian-beam Rytov phase to the signals registered by the measuring apparatus. Since $\Omega \ll \omega_0$, measurement of ψ_s requires the carrier frequency to be down shifted to a range where the sidebands carrying the desired information are accessible. This is obtained by mixing with a suitable local oscillator u_{LO} in a non-linear detecting element. For a "square-law" detector contained in the plane z (we assume, for the moment, that there is no lens), the signal resulting from the sum of the field amplitudes $u_D = u_R + u_{LO}$ is given by (HOLZHAUER and MASSIG, 1978)

$$D(\mathbf{u},\zeta,t)=\frac{C}{T}\int_{t-T}^{t}\mathrm{d}t'\int_{-\infty}^{\infty}\mathrm{d}\mathbf{u}\sigma_{\mathrm{D}}(\mathbf{u},\zeta)|u_{\mathrm{D}}(\mathbf{u},\zeta,t')|^2 \tag{4.1}$$

where C is a constant proportional to the detector sensitivity, σ_{D} is the aperture function and $1/T$ is the detector bandwidth. We assume a local oscillator related to the incident field by

$$u_{\mathrm{LO}}(\mathbf{u},\zeta,t)=ru_{\mathrm{G0}}(\mathbf{u},\zeta,t)\exp\left[-j(\Omega_{\mathrm{LO}}t+\phi_{\mathrm{LO}})\right] \tag{4.2}$$

where r is the ratio of the wave amplitudes, $\Omega_{\mathrm{LO}}=\omega_0-\omega_{\mathrm{LO}}$ is the intermediate frequency (IF) and ϕ_{LO} is an arbitrary constant phase difference. Suppressing, for the moment, the explicit spatial and temporal dependences, the signal registered by a point detector is proportional to the local intensity

$$i_{\mathrm{D}}=|u_{\mathrm{D}}|^2=e_{\mathrm{G}}[r^2+\exp(2\chi_{\mathrm{G}})+2r\exp(\chi_{\mathrm{G}})\cos(\varphi_{\mathrm{G}}-\Omega_{\mathrm{LO}}t-\phi_{\mathrm{LO}})] \tag{4.3}$$

where $e_{\mathrm{G}}=\exp(\psi_{\mathrm{G0}}+\psi_{\mathrm{G0}}^{*})$ is the beam intensity profile. In the absence of a local oscillator beam ($r=0$, *homodyne detection*), only intensity fluctuations χ_{G} arising from the diffraction of the phase-perturbed incident beam are observable (e.g. shadowgraphy, far-forward scattering). On the other hand, the phase φ_{G} can be determined free of contamination from amplitude fluctuations when either χ_{G} is small (and $r\gtrsim 1$) or $\Omega_{\mathrm{LO}}\gg\Omega$ where Ω represents a typical plasma component frequency. In the latter case, φ_{G} can be recovered by standard demodulation techniques (e.g. CHOI *et al.*, 1986).

For the phase scintillation interferometer (SHARP, 1983) $\Omega_{\mathrm{LO}}=0$, $|\chi_{\mathrm{G}}|$, $|\varphi_{\mathrm{G}}|\ll 1$ and the fluctuating part of the detected signal [equation (4.3)] is proportional to

$$\tilde{i}_{\mathrm{D}}=e_{\mathrm{G}}[\chi_{\mathrm{G}}(1+r\cos\phi_{\mathrm{LO}})+\varphi_{\mathrm{G}}r\sin\phi_{\mathrm{LO}}]. \tag{4.4}$$

The constant relative phase ϕ_{LO} is usually fixed at $\pi/2$ or $3\pi/2$ to give maximum sensitivity to the perturbed phase φ_{G}. Nevertheless, unless either diffraction effects are small $|\chi_{\mathrm{G}}|\ll|\varphi_{\mathrm{G}}|$ or the local oscillator is strong $r\gg 1$, intensity variations can significantly affect the measured signal. When $|\varphi_{\mathrm{G}}|$ is not negligible, but providing the phase variation across the beam or detecting element is small, the spatial information is still carried by a term proportional to φ_{G}. Since both real and imaginary parts of ψ_{G} figure naturally in the fluctuating intensity, it is appropriate to study the properties of the complex signal

$$c=e_{\mathrm{G}}\psi_{\mathrm{G}}\equiv c_{\chi}+jc_{\varphi}. \tag{4.5}$$

Equations (4.5) and (3.11) together allow computation of the spatial evolution of the complex signal (before and following the action of a thin focussing lens) for Gaussian-beam scattering from a thin ($l\ll 1$) normally inclined plasma wave. The real (homo-

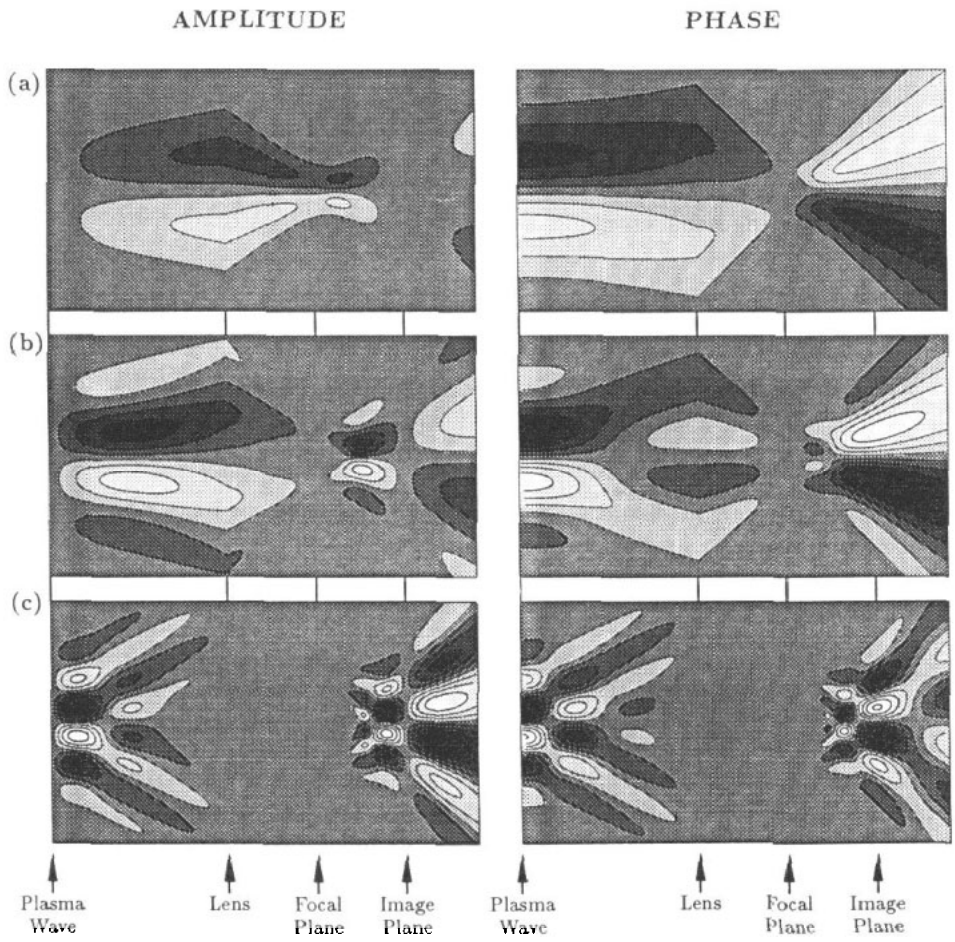

FIG. 4.—Spatial evolution of the real (left side) and imaginary (right side) parts of the complex signal $c = e_G\psi$ for Gaussian-beam scattering from a normally inclined refractive wave having (a) $\bar{k}w_0 = \pi/2$, (b) $\bar{k}w_0 = \pi$ and (c) $\bar{k}w_0 = 2\pi$. A collecting optic occupies the plane $\zeta = 0.5$ and the focal and image planes are located at $\zeta = 0.75$ and $\zeta = 1.0$, respectively.

$$n(\mathbf{R}', t) = \Delta n a(z') \cos(\bar{\mathbf{k}} \cdot \boldsymbol{\rho} - \Omega t) \tag{5.6}$$

where Δn and $a(z')$ are the perturbation amplitude and z'-distribution and $\bar{\mathbf{k}}$ is the mean transverse wavenumber. In the absence of a local oscillator beam, the detected signal is proportional to $\bar{c}_\chi = \bar{e}_G \chi_G$. Denoting by $\bar{\mathbf{v}} = \bar{\mathbf{k}} w_0$ the normalized wavevector for the plasma disturbance and $\bar{v}_\chi = -\bar{v}^2/2$, we obtain for the real and imaginary parts of $\bar{c}$

$$\bar{c}_{\substack{\chi \\ \varphi}}(\mathbf{u}, t) = \int_{-\infty}^{\infty} d\zeta' \exp[j\mathbf{u} \cdot \bar{\mathbf{v}}(\zeta' - \zeta_0)] \bar{I}_{\substack{\chi \\ \varphi}} \cos(\Omega t + \bar{\theta}_{\substack{\chi \\ \varphi}}) a(\zeta') \tag{5.7}$$

where

$$\bar{I}_{\substack{\chi \\ \varphi}} = \frac{\Delta n}{2} \exp(-\bar{\mathbf{u}}^2 + \bar{v}_F)\{\exp(2\bar{\mathbf{u}}, \bar{\mathbf{v}}) + \exp(-2\bar{\mathbf{u}} \cdot \bar{\mathbf{v}}) \mp 2\cos[2\bar{v}_F(\zeta' - \zeta_0)]\}^{1/2} \tag{5.8}$$

are the time-varying signal envelopes and the relative phases satisfy

$$\tan \bar{\theta}_\chi = \cot[(\zeta' - \zeta_0)\bar{v}_F] \frac{1 - \exp(-2\bar{\mathbf{u}} \cdot \bar{\mathbf{v}})}{1 + \exp(-2\bar{\mathbf{u}} \cdot \bar{\mathbf{v}})}$$

$$\tan \bar{\theta}_\varphi = -\tan[(\zeta' - \zeta_0)\bar{v}_F] \frac{1 - \exp(-2\bar{\mathbf{u}} \cdot \bar{\mathbf{v}})}{1 + \exp(-2\bar{\mathbf{u}} \cdot \bar{\mathbf{v}})}. \tag{5.9}$$

For a sufficiently narrow disturbance $a(\zeta') \to \delta(\zeta')$, the results of EVANS *et al.* (1982) for the homodyne signal are recovered.

When $\bar{v}_F l \ll 1$ (this *Raman–Nath* limit is discussed more fully in the next section) the quantities $\theta_\chi \to \pi/2$ and I_χ can be removed from the integral with the result

$$\bar{c}_\chi(\mathbf{u}, t) = \bar{I}_\chi \sin(\Omega t) \exp(-j\bar{\mathbf{u}} \cdot \bar{\mathbf{v}}\zeta_0) A(-\bar{\mathbf{u}} \cdot \bar{\mathbf{v}}). \tag{5.10}$$

In principle, the line-of-sight distribution $a(\zeta')$ can then be inferred from the measurements $\bar{c}_\chi$ (or $\bar{c}_\varphi$). Practically, however, the required division by the signal envelope I_χ is extremely noise prone, and limits determination of a to very low wavenumbers.

6. NEAR FIELD

We here derive the general form for the transform of the complex signal $c = e\psi_G$ in an arbitrary plane $\zeta > l$ beyond the plasma. The apodizing term is

$$e_G(\mathbf{u}; \gamma) = \frac{1}{\pi|\gamma|^2} \exp(-\mathbf{u}^2/|\gamma|^2) \tag{6.1}$$

and the Fourier transform $C(\mathbf{v}; \zeta, t) = C(\mathbf{k}; z, t)/w_0^2$ of the complex signal is given by

$$C(\mathbf{v}; \zeta, t) = jk_0 z_R \int_0^l d\zeta' \int_{-\infty}^{\infty} \frac{d\mathbf{v}'}{(2\pi)^2} E_G(\gamma\mathbf{v} - \gamma'\mathbf{v}') \exp[-j(\zeta - \zeta')\mathbf{v} \cdot \mathbf{v}'/2] N(\mathbf{v}'; \zeta', t) \tag{6.2}$$

where

$$E_G(\gamma \mathbf{v}) = \exp(-|\gamma \mathbf{v}|^2/4) \tag{6.3}$$

is the Fourier transform of e_G.

For the standard case of discrete chordal measurements, most of the beam energy is collected using a focusing lens and sensed by a single detector. Provided that $\Delta\varphi_G^2 \ll 1$ over the beam area, the detected signal is proportional to

$$\bar{i}_D(t) = \int_{-\infty}^{\infty} \mathrm{d}\mathbf{u}\sigma_D(\mathbf{u}) c_\varphi(\mathbf{u}, t). \tag{6.4}$$

(The contribution from the amplitude perturbations averaged over the beam area can be shown to vanish.) Assuming that the collecting aperture σ_D is large compared with the beam dimensions we can write with little error

$$\begin{aligned} \bar{i}_D(t) &= \mathscr{R}[C_\varphi(0;\zeta,t)] \\ &= k_0 z_R \int_0^l \mathrm{d}\zeta' \int_{-\infty}^{\infty} \frac{\mathrm{d}\mathbf{v}'}{(2\pi)^2} N(\mathbf{v}';\zeta',t)\, E_G(\gamma'\mathbf{v}') \end{aligned} \tag{6.5}$$

where C_φ is the anti-Hermitian part of C. Because of the diffraction of high-k information the probing beam acts as a low-pass filter for transmission of line-integrated refractive index information. When the plasma occupies the region within a Rayleigh length of the beam waist (*collimated beam*), the filter bandwidth is approximately spatially invariant ($\sim 2/w_0$) and the signal can be expressed as [cf. equation (6.12)]

$$\bar{i}_D(t) = -r_e \lambda_0 \int_0^L \mathrm{d}z' \hat{n}_e(0, z', t) \tag{6.6}$$

where $\hat{n}_e(0, z', t)$ is the filtered electron density on axis of the beam. Observe that this result is valid throughout the propagation region beyond the plasma. It would appear that an approximately bandlimited projection of the plasma can be obtained using a set of sufficiently closely spaced discrete probing beams. This principle is exploited in a scanning interferometer arrangement reported by HOWARD (1990).

We now consider the case when measurements are made within the collimated beam profile as with scintillation and phase contrast, or imaging interferometry experiments. For collimated beams, second-order terms in ζ and ζ' are neglected [this is a weaker condition than that leading to equation (3.10) where first-order terms in l are ignored]. This allows $E_G(\gamma\mathbf{v} - \gamma'\mathbf{v}') \to E_G(\mathbf{v} - \mathbf{v}')$ to be removed from the ζ' integral:

$$C(\mathbf{v};\zeta,t) = jk_0 z_R \int_{-\infty}^{\infty} \frac{\mathrm{d}\mathbf{v}'}{(2\pi)^2} E_G(\mathbf{v}-\mathbf{v}') \int_0^l \mathrm{d}\zeta' \exp[-j(\zeta-\zeta')\mathbf{v}\cdot\mathbf{v}'/2] N(\mathbf{v}', \zeta', t). \tag{6.7}$$

The Gaussian function significantly weights the integral for wavenumbers $|\mathbf{v}-\mathbf{v}'| \lesssim 1$. For values of $\mathbf{v}'$ satisfying this inequality the complex exponent can be approximated by noting that $\mathbf{v}\cdot\mathbf{v}' \approx \mathbf{v}^2$ provided that $|\mathbf{v}\cdot(\mathbf{v}-\mathbf{v}')| \lesssim v|\mathbf{v}-\mathbf{v}'| \lesssim v \ll v^2$ where $v = |\mathbf{v}|$. The final inequality requires the expanded beam waist to be much wider than the transverse scale length of the density variation. We refer to the region $v\zeta \equiv k_G z \ll 1$ as the *Gaussian near field*. This is distinct from the *near field* which satisfies $v^2\zeta/2 \equiv |k_F|z \ll 1$. Physically, the condition $v\zeta = k_G z \sim z/(z_R z_F)^{1/2} \ll 1$ requires substantial overlap of the main beam and diffracted orders as indicated in Fig. 3.

In the Gaussian near field of an expanded beam, equation (6.7) becomes

$$C(\mathbf{v}, \Omega; \zeta) = \mathscr{R}_G(v_F; \zeta)\hat{N}(\mathbf{V}_F, \Omega) \tag{6.8}$$

where $\mathbf{V}_F = (\mathbf{v}, v_F)$ and $\hat{N} = (N * E_G)/(2\pi)^2$ is proportional to the two-dimensional convolution of N with E_G. The parabolic approximation to the Gaussian-beam Rytov-phase propagator is given by [cf. equation (2.23)]

$$\mathscr{R}_G(v_F; \zeta) = jk_0 z_R \exp(jv_F\zeta). \tag{6.9}$$

In the spatial domain, the measured signal is proportional to the plane-wave Rytov phase weighted by the Gausian-beam intensity profile [cf. equation (2.22)]. For separable $N(\mathbf{v}; \zeta', t) = N'(\mathbf{v}; t)a(\zeta')$ and provided $v \gg 1$, equation (6.7) becomes

$$C(\mathbf{v}; \zeta, t) = \mathscr{R}_G(v_F; \zeta)\hat{N}'(\mathbf{v}; t)A(v_F) \tag{6.10}$$

where $\hat{N}' = (N' * E_G)/(2\pi)^2$ is defined analogously to $\hat{N}$ and $A(v_F)$ is the Fourier transform of $a(\zeta')$. Knowledge of $\hat{N}'$ then allows $a(\zeta')$ to be determined to a band-limit such that division by $\hat{N}'$ does not prohibitively amplify noise on the measured spectrum C.

Let us consider the case of a quasi-monochromatic density perturbation propagating normal to the laser beam. As indicated schematically in Fig. 5, the spatially localized beam presents a spread of incident wavenumbers $\Delta k_x \sim 2/w_0$ that sample the source transform over the range $\Delta k_z \sim (K/k_0)\Delta k_x$. The scattered waves are conveyed according to the strength of the transform $N(\mathbf{K}, \Omega)$ at the intersection with the circular arc defining the locus of allowable scattered wave vectors. Since the spectral width $\Delta k_A \sim 2\pi/L$ represents the minimum distance over which A can change significantly, the narrower the structure the greater will be the range of its transform in the k_z direction. It is therefore sufficient that the Klein–Cook parameter (KLEIN and COOK, 1967) $Q = |k_F|L$ be small for the density wave to be sensed by the probing radiation. This is ensured when the phase screen is sufficiently thin (Raman–Nath regime). Otherwise the incident beam must be inclined in order that **k**-matching be satisfied (Bragg regime). Determination of A to the bandwidth Δk_A requires $(K/k_0)\Delta k_x \gtrsim 2\pi/L$. Since the beam is collimated ($L \ll z_R$) we therefore have $1 \ll Kw_0 \lesssim Q$ so that, for collimated beams, the scattering must be performed in the Bragg regime in order that the z-distribution of the source be recovered.

In the *geometric optics* limit we approximate $\mathscr{R}_G(v_F; \zeta) \approx jk_0 z_R(1 + jv_F\zeta)$. Since $\zeta > l$, the geometric optics limit implies Raman–Nath diffraction where the transform

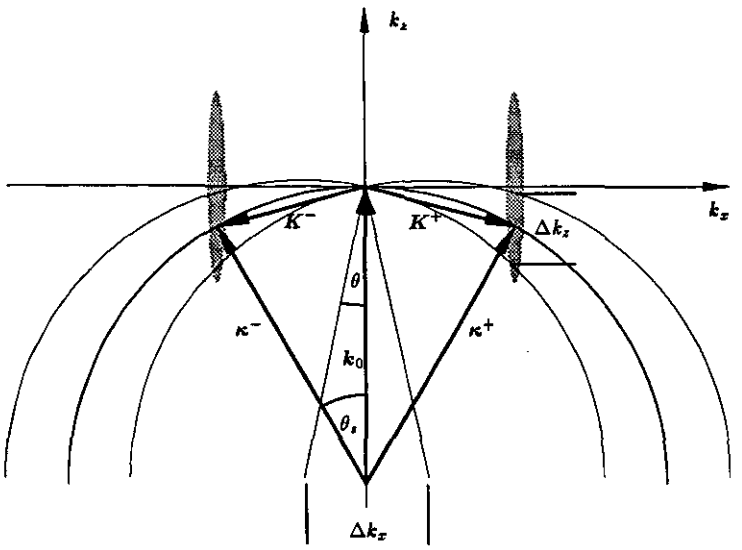

FIG. 5.—Schematic diagram showing satisfaction of the k-matching condition for Gaussian-beam scattering from the quasi-coherent plasma perturbation whose domain in the Fourier transform plane is shaded. An incident k-spread Δk_x maps the transform over the range Δk_z.

$\hat{N}$ can also be approximated to first order:

$$\hat{N}(\mathbf{V}_F, \Omega) \approx \int_0^l d\zeta'(1 - jv_F\zeta')\hat{N}(\mathbf{v}, \Omega; \zeta'). \tag{6.11}$$

With these expansions, inverse Fourier transformation over $\mathbf{v}$ and Ω gives

$$c \approx jc_\varphi(\boldsymbol{\rho}/w_0, t) = -jr_e\lambda_0 e_G(\boldsymbol{\rho}/w_0; \gamma) \int_0^L dz' n_e(\boldsymbol{\rho}, z', t) \tag{6.12}$$

where higher-order terms have been neglected. The result is valid in the Rytov approximation which, assuming the medium varies smoothly, can be written as $\varphi_G \ll k_0 L$ where the right-hand side is the phase shift of the unperturbed wave. In absolute terms, the phase φ_G can be large. Gaussian near-field and geometric optics conditions can often be ensured using imaging techniques (HUGENHOLTZ and MEDDENS, 1982; YOUNG *et al.*, 1984; HOWARD *et al.*, 1987; NAZIKIAN and SHARP, 1987). When the beam is allowed to freely propagate before being sensed by an array of detectors (e.g. PEEBLES *et al.*, 1987; KIM *et al.*, 1988) however, the effects of propagation ($\mathscr{R}_F$) must be carefully assessed (HOWARD *et al.*, 1990).

6.1. *Diffraction from waves*

To compare with the results of scintillation experiments presented in Section 7, we apply equation (6.7) to obtain the near- and intermediate-field behaviour for laser

diffraction from density waves. We assume the sound field takes the form of equation (5.6) with $\bar{\mathbf{v}} = \bar{\mathbf{k}} w_0$. Substitution into equation (6.7) and separating c into real and imaginary parts gives

$$c_{\varphi}^{\chi}(\mathbf{u}, \zeta) = \int_0^{\zeta} \mathrm{d}\zeta' a(\zeta') I_{\varphi}^{\chi} \cos(\Omega t + \theta_{\varphi}^{\chi}) \tag{6.13}$$

where

$$I_{\varphi}^{\chi} = \frac{\Delta n}{2} \exp[-\mathbf{u}^2 - \beta_i \bar{v}_F(\zeta - \zeta')] \{\exp(2\beta_i \mathbf{u} \cdot \bar{\mathbf{v}}) + \exp(-2\beta_i \mathbf{u} \cdot \bar{\mathbf{v}}) \mp 2\cos[2\beta_r \bar{v}_F(\zeta - \zeta')]\}^{1/2}, \tag{6.14}$$

$$\tan\theta_{\chi} = \frac{\cos(u_+) - \exp(2\beta_i \mathbf{u} \cdot \bar{\mathbf{v}})\cos(u_-)}{\sin(u_+) + \exp(2\beta_i \mathbf{u} \cdot \bar{\mathbf{v}})\sin(u_-)}$$

$$\tan\theta_{\varphi} = -\frac{\sin(u_+) - \exp(2\beta_i \mathbf{u} \cdot \bar{\mathbf{v}})\sin(u_-)}{\cos(u_+) + \exp(2\beta_i \mathbf{u} \cdot \bar{\mathbf{v}})\cos(u_-)} \tag{6.15}$$

with

$$\beta = \beta_r + j\beta_i$$

$$u_{\pm} = \beta_r \bar{v}_F(\zeta - \zeta') - \beta_r \mathbf{u} \cdot \bar{\mathbf{v}}. \tag{6.16}$$

In the far-field limit, and with the identification $\varepsilon \equiv \zeta - \zeta'$, equation (6.13) reduces to its Fraunhofer counterpart equation (5.7) (see also the Appendix).

For a collimated laser beam $\beta \to 1 - j(\zeta - \zeta')$ and for a localized perturbation ($L \ll z_R$), the above result reduces to a simple form obtainable directly from equation (3.10). For the Gaussian amplitude distribution

$$a(z) = (2\pi)^{-1/2} \exp[-z^2/(2L^2)] \tag{6.17}$$

($L \ll z_R$) and monochromatic sound field $\bar{\mathbf{k}} = (\bar{k}, 0)$ [see equation (5.6)], it can be established that

$$c = e_G \psi_P = j\Phi e_G(\mathbf{u}; \gamma) \exp(-Q^2/2) \cos(\bar{v}u - \Omega t) \exp(j\bar{v}_F \zeta) \tag{6.18}$$

where $\Phi = k_0 L \Delta n \equiv -\lambda_0 r_e L \Delta n_e$ is the absolute phase perturbation. Using the above, we can readily obtain explicit expressions for the heterodyne and homodyne signal envelopes and relative phases for comparison with experiment. Finally, for a thin phase screen ($Q \ll 1$), the real part of equation (6.18) reduces to the near-field expression obtained by JAMES and YU (1985) for Gaussian beam scattering from waves.

7. SCINTILLATION EXPERIMENTS

The scintillation diagnostic is a high-sensitivity Mach–Zehnder imaging interferometer that operates in the near-field (Raman–Nath) regime and is specifically designed for the detection of high spatial and temporal frequency plasma density induced phase and amplitude fluctuations. The instrument uses an expanded Gaussian beam ($w_0 \sim 10$ mm) of 10.6 μm radiation for heterodyne and homodyne scintillation measurements of airborne ultrasound. The measurement system layout is shown in Fig. 6.

The optical system (consisting of a 10 W gas-discharge CO_2 laser, beam-expansion optics and interferometer components) is mounted on a massive marble table and the sound source is a standard tweeter (cooled to -5°C) driven by an audio amplifier (300 W rms). Anti-reflection-coated 7.5 cm diameter ZnSe 50% beamsplitters are used to separate and combine the probing and local oscillator beams. The local oscillator is thus nominally identical to the probing beam apart from a constant phase offset

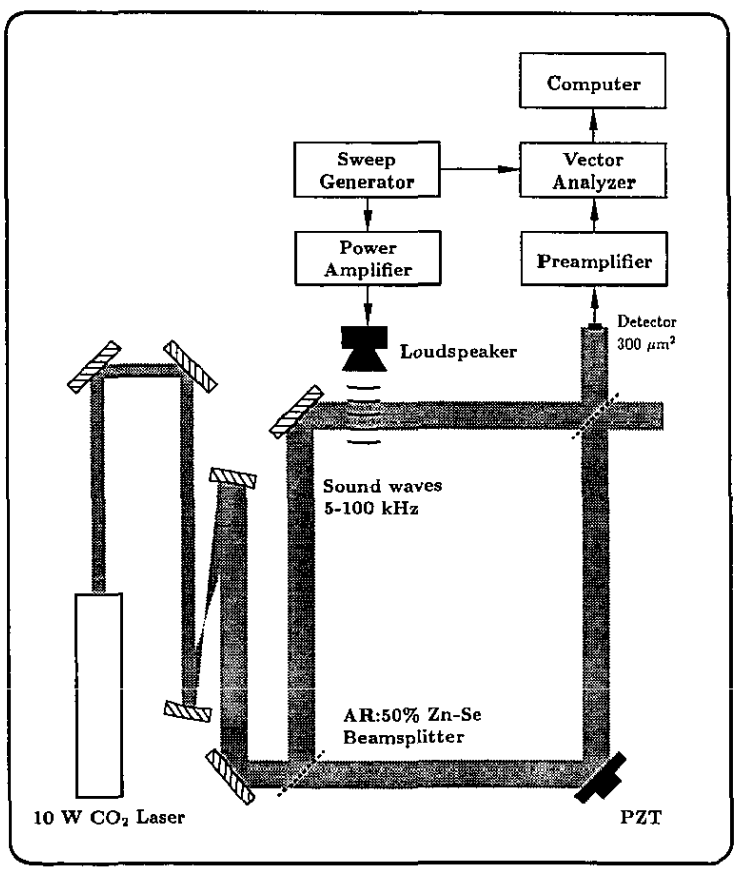

FIG. 6.—Schematic diagram of scintillation interferometer for ultrasonic wave measurements. PZT denotes the peizo-driven mirror used for fixing the relative path lengths between the interferometer arms.

held at $\phi_{LO} \simeq \pi/2$ by the peizo-controlled mirror in the interferometer reference arm. The Rayleigh length $z_R \sim 40$ m is much greater than the sound screen thickness $L \sim 0.005$ m so that the Rytov-phase perturbation is given to sufficient accuracy by equation (3.10). The perturbed field propagates to the detector plane located at a distance $z = 2.10$ m from the interaction region. Up to two Fresnel zones are accessible by scanning the sound frequency from 5 kHz to a maximum of 100 kHz. On the other hand, the sound field remains strongly Raman–Nath even at the maximum sound frequency ($Q = |\bar{k}_F|L \sim 0.15$).

A single Hg–Cd–Te detector of dimensions 300×300 μm (located on the axis of

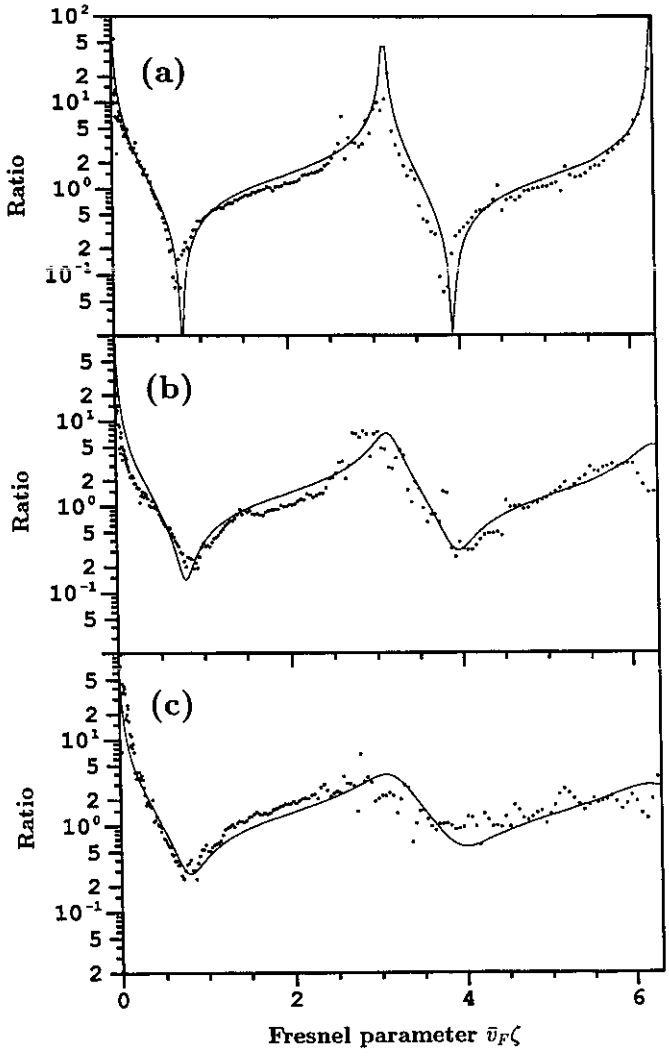

FIG. 7 (a)–(c).—The experimental (dotted) and computed (solid) ratios of the heterodyne and homodyne signals versus the Fresnel parameter $Q = v_F\zeta$ for detector positions $x = 0$, 3 and 6 mm from the Gaussian-beam centre.

the beam) is used for these measurements. Using synchronous detection techniques (integration time 1 s), the interferometer is capable of sensing phase shifts as small as $\sim 10^{-5}$ radians. The homodyne and heterodyne signal amplitudes are measured in turn and digitized for later processing by computer.

As noted above, the Fresnel parameter $\bar{v}_F\zeta$ is varied by changing the frequency of the sound waves. The experimental points and theoretical curves for the variation of the ratio of heterodyne and homodyne signal amplitudes with $\bar{v}_F\zeta$ measured at $x = 0$, 3 and 6 mm from the beam centre are shown in Fig. 7. The ratio is taken to remove the dependence on the system frequency response. The decrease in signal-to-noise ratio at higher Q values is due to the decrease by an order of magnitude in speaker efficiency. The nominal experimental parameters are: sound speed $C_s = 330 \pm 5\ \mathrm{m\ s^{-1}}$, $r = 1.0 \pm 0.05$, $\phi_{LO} = -90° \pm 5°$, $w_0 = 11 \pm 1$ mm and $z = 2.10 \pm 0.02$ m. Systematic discrepancies are possibly attributable to a small mismatch of local oscillator and probe beams. We also note that a slightly closer fit with experiment can usually be obtained by the appropriate choice (within the quoted uncertainty bounds) of the above parameter values. The sensitivity to screen thickness L and waist position z_0 (within a Rayleigh range) is, however, weak.

The general agreement over three orders of magnitude confirms the functional behaviour described by equation (6.18). The variation with x highlights the importance of finite beam effects for high-resolution near-field scattering measurements. Based on the measurements of Fig. 7(a) we conclude that near field ($v_F\zeta < 1$) measurements of the complex signal should be sufficient to locate a narrow, coherent source with an accuracy of $\sim 5\%$. Experiments examining other parameter dependences, and in which both phase and amplitude response are measured, are underway.

Acknowledgements—The authors wish to thank R. N. NAZIKIAN for useful discussions and S. M. HAMBERGER for provision of the facilities necessary for this research.

REFERENCES

BANOS A. (1966) *Dipole Radiation in the Presence of a Conducting Half Sphere*. Pergamon, Oxford.
CHOI D. W., POWERS E. J., BENGSTON R. D., JOYCE G., BROWER D. L., LUHMANN N. C., JR and PEEBLES W. A. (1986) *Rev. Scient. Instrum.* **57**, 1989.
CLIFFORD S. F. (1978) in *Laser Beam Propagation in the Atmosphere* (Edited by J. W. STROHBEHN), p. 10. Springer, New York.
DEVANEY A. J. (1986) *Inverse Problems* **2**, 161.
EVANS D. E., VON HELLERMAN M. and HOLZHAUER E. (1982) *Plasma Phys.* **24**, 819.
GOODMAN J. W. (1968) *Introduction to Fourier Optics*. McGraw-Hill, San Fransisco.
HOLZHAUER E. and MASSIG J. H. (1978) *Plasma Phys.* **20**, 867.
HOWARD J. (1990) *Rev. Scient. Instrum.* **61**, 1086.
HOWARD J., DOYLE E. J., REIBIZ G., SAVAGE R. L., PEEBLES W. A., GULL S. F. and LUHMANN N. C., JR (1987) *Proc. 14th European Conf. on Controlled Fusion and Plasma Physics* (Edited by G. Thomas), p. 1310. EPS, Geneva.
HOWARD J., PEEBLES W. A., BROWER D. L., KIM S. K. and LUHMANN N. C., JR (1990) *Rev. Scient. Instrum.* **61**, 2829.
HUGENHOLTZ C. A. J. and MEDDENS B. J. H. (1982) *Rev. Scient. Instrum.* **53**, 171.
JACOBSON A. R. (1982) *Plasma Phys.* **24**, 1111.
JAMES B. W. and YU C. X. (1985) *Plasma Phys. Contr. Fusion* **27**, 557.
KAK A. C. (1985) in *Array Signal Processing* (Edited by S. HAYKIN). Prentice-Hall, New Jersey.
KIM S. K., BROWER D. L., PEEBLES W. A. and LUHMANN N. C., JR (1988) *Phys. Rev. Lett.* **60**, 577.
KLEIN W. R. and COOK W. D. (1967) *IEEE Trans. Sonics Ultrasonics*, **SU-14**, 123.
MUELLER R. K., KAVEH M. and IVERSON R. D. (1980) *Acoust. Imag.* **8**, 615.
NAZIKIAN R. (1989) Interferometric study of density fluctuations in a Tokamak plasma. Thesis, A.N.U.
NAZIKIAN R. and SHARP L. E. (1987) *Rev. Scient. Instrum.* **58**, 2086.

PAPOULIS A. (1986) *Systems and Transforms with Applications in Optics*, pp. 322–323. Robert E. Krieger Publishing Company, Malabar, Florida.
PEEBLES W. A., SAVAGE R. L., JR, BROWER D. L., KIM S. K., LEHECKA T., HOWARD J., DOYLE E. J. and LUHMANN N. C., JR (1987) *Int. J. Infrared Millimeter Waves* **8**, 1355.
SHARP L. E. (1983) *Plasma Phys. Contr. Fusion* **25**, 781.
SHEFFIELD J. (1975) *Plasma Scattering of Electromagnetic Radiation*. Academic Press, New York.
SHEWELL J. R. and WOLF E. (1968) *J. Opt. Soc. Am.* **58**, 1596.
SLANEY M., KAK A. C. and LARSEN L. E. (1984) *IEEE Trans. Microwave Theory Tech.* **MTT-32**, 860.
STROHBEHN J. W. (1968) *Proc. IEEE* **56**, 1301.
SURKO C. M. and SLUSHER R. E. (1980) *Physics Fluids* **23**, 2425.
WEISEN H., HOLLENSTEIN CH. and BEHN R. (1988) *Plasma Phys. Contr. Fusion* **30**, 293.
WOLF E. (1969) *Opt. Commun.* **1**, 153.
YOUNG P. E., NEIKIRK D. P., TONG P. P., RUTLEDGE D. B. and LUHMANN N. C., JR (1984) *Rev. Scient. Instrum.* **56**, 81.

APPENDIX : DIFFRACTION PROJECTION THEOREM AND THE PARABOLIC APPROXIMATION

The diffraction projection theorem (WOLF, 1969) is the reciprocal space solution to the inhomogeneous wave equation in the first Born approximation. For the special case of plane-wave illumination, and in the limit of zero wavelength, the result reduces to the well-known "central slice" theorem for non-diffracting tomographic imaging. The proof of the theorem, which we sketch below, rests on the assumption that the scattering is weak in the Born sense. More comprehensive treatments are given by WOLF (1969), MUELLER *et al.* (1980), KAK (1985) and DEVANEY (1986).

The Green's function is the spherical-wave solution to the wave equation for a point source. The spherical wave has the plane-wave decomposition [BANOS, 1966; cf. equation (2.6)]:

$$g(\mathbf{R}-\mathbf{R}') = \frac{-j}{2}\int_{-\infty}^{\infty}\frac{\mathrm{d}\boldsymbol{\kappa}_\perp}{(2\pi)^2\kappa_z}\exp\{j[\boldsymbol{\kappa}_\perp\cdot(\boldsymbol{\rho}-\boldsymbol{\rho}')+\kappa_z|z-z'|]\}. \tag{A.1}$$

The above expression for g is inserted into equation (2.12), and since f_0 is zero for $z > L$, we replace $|z-z'|$ by $z-z'$ to obtain after some rearrangement

$$u_s(\mathbf{R},t) = j\int_{-\infty}^{\infty}\frac{\mathrm{d}\boldsymbol{\kappa}_\perp}{(2\pi)^2\kappa_z}\exp(j\boldsymbol{\kappa}\cdot\mathbf{R})\int_{-\infty}^{\infty}\mathrm{d}\mathbf{R}' f_0(\mathbf{R}',t)\exp(-j\boldsymbol{\kappa}\cdot\mathbf{R}'). \tag{A.2}$$

Recognizing the rightmost integral as the Fourier transform F_0 of the scattering potential, the scattered field can be more compactly expressed as

$$u_s(\mathbf{R},t) = j\int\!\!\int_{-\infty}^{\infty}\frac{\mathrm{d}\boldsymbol{\kappa}_\perp\,\mathrm{d}\omega}{(2\pi)^3\kappa_z}\exp[j(\boldsymbol{\kappa}\cdot\mathbf{R}-\omega t)]F_0(\boldsymbol{\kappa},\omega). \tag{A.3}$$

Fourier transformation over $\boldsymbol{\rho}$ and t yields the desired result (2.14).

In the parabolic approximation u_s can be cast in a Fresnel integral form similar to equation (2.5) for the free space field. We prefer, however, to represent the scattered field as the superposition of beams identical to the incident field but diffracted from the medium at angles determined by the spectrum of the scatterer. In the parabolic approximation the trajectory of the plane-wave component $(0,0,k_0)$ of the incident field diffracted from the perturbation $\mathbf{K}_F = (\mathbf{k}, k_F)$ is

$$\boldsymbol{\rho}' = \boldsymbol{\rho} - \frac{\mathbf{k}}{k_0}(z-z') \tag{A.4}$$

where z' is the coordinate in the plasma. Applying the convolution theorem in equation (A.2) isolates the three-dimensional Fourier transform U_0 of the incident field:

$$u_s(\mathbf{R},t) = jk_0^2\int_{-\infty}^{\infty}\frac{\mathrm{d}\mathbf{K}\,\mathrm{d}\omega}{(2\pi)^4}N(\mathbf{K},\Omega)\int_{-\infty}^{\infty}\frac{\mathrm{d}\boldsymbol{\kappa}_\perp}{(2\pi)^2\kappa_z}\exp[j(\boldsymbol{\kappa}\cdot\mathbf{R}-\omega t)]U_0(\boldsymbol{\kappa}-\mathbf{K}). \tag{A.5}$$

Substituting for U_0

$$U_0(\boldsymbol{\kappa}) = 2\pi A_0(\boldsymbol{\kappa}_\perp; 0)\delta[\kappa_z - (k_0^2 - \boldsymbol{\kappa}_\perp^2)^{1/2}], \tag{A.6}$$

transforming to trajectory coordinates ρ' and integrating then gives (NAZIKIAN, 1989)

$$u_s(\mathbf{R}, t) = \int_0^L \mathrm{d}z' \int_{-\infty}^{\infty} \frac{\mathrm{d}\boldsymbol{\kappa}\,\mathrm{d}\omega}{(2\pi)^3} \exp(j\boldsymbol{\kappa}\cdot\boldsymbol{\rho})\mathscr{R}_F(k_F; z-z')N(\mathbf{k}, \Omega; z')u_0(\boldsymbol{\rho}', z)\exp(-j\omega t) \tag{A.7}$$

where $N(\mathbf{k}, \Omega; z')$ is the 1-D inverse Fourier transform of $N(\mathbf{K}, \Omega)$ and $\mathscr{R}_F$ is the parabolic approximation to the plane-wave propagator $\mathscr{R}$ [equation (2.23)]. This shows that for each density spectral component $N(\mathbf{k}, \Omega; z')$ there is a diffracted wave $u_0(\boldsymbol{\rho}', z)\exp(-j\omega t)$, identical in form to the incident field, and that the field u_s is the propagation-weighted superposition of all such contributions. More importantly, the result provides a useful representation for the Rytov phase:

$$\psi_s(\mathbf{R}, t) = \int_0^L \mathrm{d}z' \int_{-\infty}^{\infty} \frac{\mathrm{d}\boldsymbol{\kappa}}{(2\pi)^2} \exp(j\boldsymbol{\kappa}\cdot\boldsymbol{\rho})\mathscr{R}_F(k_F; z-z')N(\mathbf{k}; z', t)\exp[\psi_0(\boldsymbol{\rho}', z) - \psi_0(\boldsymbol{\rho}, z)]. \tag{A.8}$$

The Gaussian-beam Rytov phase ψ_G is obtained easily on substitution for the unperturbed phase ψ_{G0} from equation (3.3). The expression also has some nice properties that facilitate calculation of ψ_s in the far-field limit.

Transition to the far field

Equation (A.8) can be recast in the form

$$\psi_s(\mathbf{R}, t) = jk_0 \int_0^L \mathrm{d}z' \exp(j\sigma^2\boldsymbol{\rho}^2/2) \int_{-\infty}^{\infty} \frac{\mathrm{d}\boldsymbol{\kappa}}{(2\pi)^2} \exp(-j\sigma^2\boldsymbol{\rho}'^2/2)N(\mathbf{k}; z', t)\exp[\psi_0(\boldsymbol{\rho}', z) - \psi_0(\boldsymbol{\rho}, z)] \tag{A.9}$$

where $\sigma^2 = k_0/(z-z')$. For the *plane wave* $(0, 0, k_0)$, the final term is unity. In the far field, $\sigma^2 \simeq k_0/z \to 0$ and the complex exponential in the second integral tends to the impulse $-2\pi j\sigma^2\delta(\boldsymbol{\rho}')$ (PAPOULIS, 1986) with the result

$$\begin{aligned} \bar{\psi}_s(\mathbf{R}, t) &= \lim_{\sigma^2 \to \infty} \psi_s(\mathbf{R}, t) \\ &= \frac{1}{\lambda_0} \int_0^L \mathrm{d}z' \sigma^2 \exp(j\sigma^2\boldsymbol{\rho}^2/2)N(\sigma^2\boldsymbol{\rho}; z', t). \end{aligned} \tag{A.10}$$

Retaining terms $\sigma^2 \simeq (1+z'/z)k_0/z$ in the exponent and taking $\sigma^2 \simeq k_0/z$ elsewhere, we finally obtain

$$\bar{\psi}_s(\mathbf{R}, t) = r_F(\boldsymbol{\rho}, z)N(\mathbf{K}_F; t) \tag{A.11}$$

where, with the correspondence $\mathbf{k} = (k_0/z)\boldsymbol{\rho}$, $\mathbf{K}_F$ is the Fresnel wave vector introduced above, and

$$r_F(\boldsymbol{\rho}, z) = jk_0 \exp(-jk_0 z)h_F(\boldsymbol{\rho}, z) \tag{A.12}$$

is the Fourier transform of the parabolic plane-wave propagator $\mathscr{R}_F$.

For *Gaussian beams*, and in terms of the dimensionless quantities introduced in Section 3, the Rytov phase is given by

$$\psi_s(\mathbf{u}, \zeta, t) = jk_0 z_R \int_0^{\zeta} \mathrm{d}\zeta' \exp[\beta\tilde{\mathbf{u}}^2(\zeta-\zeta')/2] \int_{-\infty}^{\infty} \frac{\mathrm{d}\mathbf{v}}{(2\pi)^2} \exp[-\beta(\tilde{\mathbf{u}}-\mathbf{v})^2(\zeta-\zeta')/2]N(\mathbf{v}; \zeta', t) \tag{A.13}$$

where

$$\tilde{\mathbf{u}} = \frac{\mathbf{u}}{\zeta - \zeta'} \tag{A.14}$$

is analogous to the focal-plane coordinate defined in Section 5. Performing the ζ' integration in the far-field limit, we find

$$\bar{\psi}_s(\mathbf{u}, \zeta, t) = jk_0 z_R \exp(\gamma_0 \bar{\mathbf{u}}^2/2) \int_{-\infty}^{\infty} \frac{d\mathbf{v}}{(2\pi)^2} \exp[-\gamma_0(\bar{\mathbf{u}}-\mathbf{v})^2/2] N(\mathbf{v}, -\bar{\mathbf{u}}\cdot\mathbf{v} - v_F; t) \tag{A.15}$$

where, as usual, $v_F = -\mathbf{v}^2/2$. With the correspondence $\varepsilon \equiv \varepsilon'$, the far-field and focal-plane expressions for the complex signal $c = e_G \psi_s$ are identical.